Manufacturing Science and Technology 3(5): 286-293, 2015
DOI: 10.13189/mst.2015.030515 http://www.hrpub.org

Electrochemical Corrosion Behavior of Spirally-welded API X-70 Line-pipe Steel in Acidic and Salt Media

Sohail M. A. Khan[2], Asiful H. Seikh[1,*], Muneer Baig[1], Magdy M. El Rayes[2]

[1]Centre of Excellence for Research in Engineering Materials (CEREM), Advanced Manufacturing Institute, King Saud University, Saudi Arabia
[2]Department of Mechanical Engineering, College of Engineering, King Saud University, Saudi Arabia

Abstract The electrochemical behavior of spirally-welded API steel was investigated at ambient temperature in 3.5% NaCl and 1M H_2SO_4 solution using linear polarization and electrochemical impedance spectroscopy (EIS) techniques. In order to reveal the corrosion resistance of different regions within the welded joint some significant characterization parameters in linear polarization and EIS curves were analyzed and compared. The surface morphology of corrosion products was also analyzed by scanning electron microscopy (SEM) and energy-dispersive spectrometer (EDS). The results showed that the corrosion resistance of the steel in both solutions at ambient temperature follows the order Weld Metal - Base Metal and HAZ. The corrosion of welded steel in sulfuric acid solution is more than that in NaCl solution.

Keywords Welded Line-pipe Steels, Polarization, Electrochemical Impedance Spectroscopy, Corrosion Resistance

1. Introduction

Carbon steels are the most important alloys used in petroleum and chemical industries since they account for over 98% of the construction materials. Of all the carbon steels, low carbon steels are widely used in oil / gas storage tanks and transportation pipelines because they display significant ductility, good weldability characteristics and possess reasonable strength and toughness [1-3]. However, these welded structures (pipe-lines, off-shore rigs, agitators, pumps, tanks etc.) are subjected to severe corrosion due to the aggressive chemical solutions [4-6] loaded with impurities (chlorides, sulphates etc.) [7-9].

Generally, a welded joint is composed of three zones with different corrosion behaviors: base metal (BM), heat-affected zone (HAZ) and weld metal (WM). The HAZ can be severely affected due to the metallurgical changes caused by welding thermal cycles. The HAZ is the most sensitive region that is prone to corrosion due to the precipitation of chromium carbides [10, 11], which is of important concern in maintaining the integrity of pipelines, cylinders and tanks [12].

The steel pipe used for oil and gas transport are manufactured by welding different segments of carbon steel which alters the microstructure of the materials by causing local variations in the composition and phases. The difference in chemical composition, metallurgical phases, microstructure and mechanical performance of these pipe-line steels may result in the varied corrosion behaviors. These changes increase the dissimilarity of the base/weld metal combination and can cause galvanic corrosion [13]. Therefore, weldment corrosion in various industrial media attributes much attention, and different results have been reported depending on the base metal, corrosive media and welding technology [14-17]. Earlier published work [18-22] suggests that corrosion is more severe in the contact region between the base and the welded zones. This is mainly due to the galvanic corrosion between the base and the weld metals. It should be noted that significant number of studies on the electrochemical corrosion of pipe-line steel is mainly focused on the stress cracking corrosion (SCC). Thus, it is imperative to understand the corrosion behavior of welded API pipe-line steel in view of the extensive and perdurable application. The aim of this work is to investigate the corrosion behavior of spirally welded API pipe-line steel in 3.5% NaCl and 1M H_2SO_4 solutions using linear polarization and electrochemical impedance spectroscopy techniques. The surfaces of the samples were characterized using SEM analysis and EDX techniques.

2. Experimental

2.1. Materials Preparation

The weld materials used in this study were produced by

sub-merged arc welding (SAW) process with 2.5 mm diameter-welding wire classified as high Mn welding electrodes according to the American Welding Society code (AWS A5.17) and also (ASTM A558). According to the same classification code the flux used was F71 type which is compatible to the welding wire composition. The material used in this investigation was as received spirally welded pipe. Three different zones i.e., BM, WM and HAZ were studied individually and compared. The specimen for electrochemical tests was cut in to 10 × 10 × 5 mm dimension from three different zones. The chemical composition of specimens from different zones is presented in Table 1. Specimens were degreased with acetone, air dried and embedded into two-component epoxy resin and mounted in a glass holder. The specimens were later embedded in two component epoxy resin in a glass holder, leaving a rectangular cross section area of 1 sq. cm acts as working electrode. The coupons were degreased with acetone, A copper wire was soldered to the rear side of the coupon which works as counter/ reference electrode. Prior to each experimental run, the exposed surface of the working electrode (of area 100 mm^2) was wet polished with 1000 grit silicon carbide, rinsed with ethanol and air dried.

2.2. Optical Microscopy

One of the surfaces of the each metallographic specimens BM, WM and HAZ were mechanically ground on the silicon carbide abrasive papers sequentially on 60, 120, 240, 320, 400, 600 grit silicon carbide papers and polished on a Sylvet cloth using coarse and fine Geosyn- Grade I slurry of Al_2O_3. Specimens were cleaned in water, alcohol and then dried in air. All the polished specimens were etched using 2% Nital solution (2% HNO_3 in Ethanol). The etched specimens were observed by XJL-03 model metallographic microscope.

2.3. Solution Preparation

Experiments were done in stagnant 3.5% NaCl and 1M H_2SO_4 solution. All solutions were prepared from analytical grade reagents and distilled water. While the electrolyte solutions were in equilibrium with the atmosphere, all experiments were carried out under thermostatic conditions 25^oC (±0.1^oC).

2.4. Experimental Procedure (Linear Polarization and the EIS)

Electrochemical experiments were performed in a conventional three-electrode cell in which Ag/AgCl was the reference electrode, platinum foil was the counter electrode whereas the API steel was the working electrode (WE). All potentials quoted in this paper were referred to the Ag/AgCl. The area of the WE exposed to the solution was 1 cm^2. The electrochemical experiments were performed by Autolab Potentiostat (PGSTAT20 computer controlled) operated by the general purpose electrochemical software (GPES) version 4.9. The free corrosion potential (versus Ag/AgCl) was followed after immersing the working electrode in the test solution until the potential stabilized within ±1mV. This was followed by electrochemical impedance spectroscopy test. EIS data were recorded for the weld specimens at corrosion potentials (E_{corr}) immersed in the test solution. The frequency was scanned from 100 KHz to 100 MHz, with an ac wave of ± 5 mV peak-to-peak overlaid on a dc bias potential to get Nyquist and bode plots. The best equivalent circuit of Nyquist plots was calculated by fit and simulation method. The linear potentiodynamic polarization curves were obtained by scanning the potential in the forward direction from −0.25 to 0.25V against Ag/AgCl at a scan rate of 1 mV/s.

All the electrochemical experiments were recorded after immersion of the electrode in the test solution at a temperature of (25±1)^0C. Fresh solution and fresh specimens were used after each weep. For each experimental condition, two to three measurements were performed to ensure the reliability and reproducibility of the data.

2.5. Characterization of Surface Films

The morphology of the corroded surface of each specimen were analyzed using a FE SEM [JEOL model JSM-6610LV – Japan] with an energy dispersive X-ray analyzer attached for acquiring the EDX analysis. The specimens were washed and dried after being withdrawn from the test cell to enable the characterization of adherent corrosion products with no residues.

Table 1. Chemical composition of spiral welded steel.

	C	Si	Mn	P	S	Cu	Ni	Ti	V	Nb
WM	0.109	0.229	1.67	<0.0005	<0.0005	0.0434	0.017	0.102	0.0297	0.0269
HAZ	0.114	0.235	1.52	<0.0005	<0.0005	0.0267	0.0147	0.0167	0.0463	0.0500
BM	0.11	0.226	1.48	<0.0005	0.0008	0.0264	0.0145	0.0156	0.045	0.0471

3. Results

3.1. Metallography of the Welded Joint

In general, the weldment shown is composed of WM, also known as fusion zone, the (HAZ), and the unaffected base metal (BM). The BM microstructure is shown in Fig. 1 which is composed of a ferritic matrix with pearlite in which the ferrite is the dominant phase leading to enhanced weldability and satisfactory strength. Although the WM and base metals have almost the same composition based on carbon equivalent calculations, the WM microstructure however is noticeably different from the HAZ as well as the unaffected base metal. This difference is noted while comparing the microstructures of the WM in its as-deposited condition (as-cast structure) and the BM. The WM experiences melting and solidification, and its microstructural characteristics can be described as columnar structure of mainly acicular ferrite and proeutectoid ferrite at grain boundary as shown in Fig. 2. The HAZ exhibited coarsened grains of ferrite. The coarse-grained microstructure is within the HAZ and is adjacent to the fusion line (boundary) of WM which has been subjected to peak temperatures leading to grain coarsening as shown at higher magnification in Fig. 3.

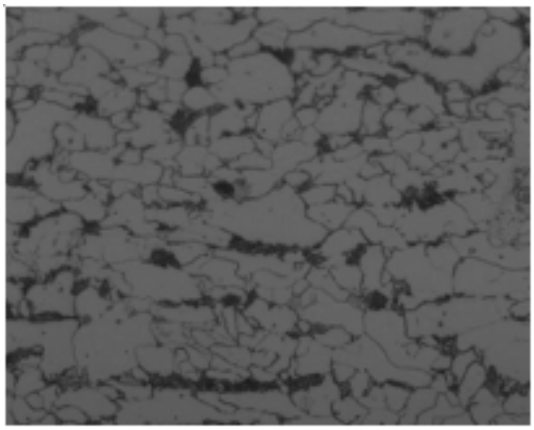

Figure 1. Unaffected base metal at x100 magnifications

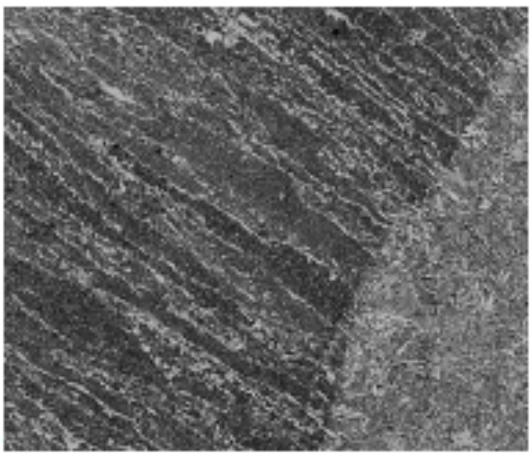

Figure 2. The fusion line (FL) separating the weld metal

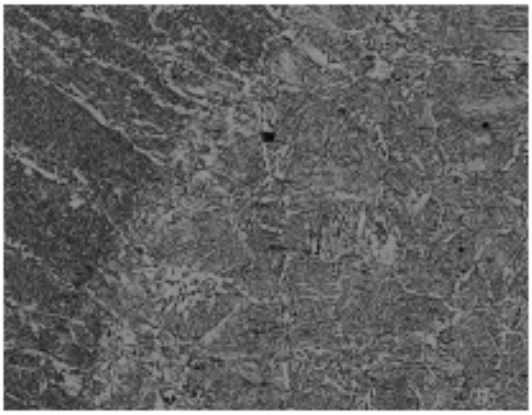

Figure 3. Coarse-grained supercritical HAZ at higher magnification

3.2. Potentiodynamic Polarization Curves

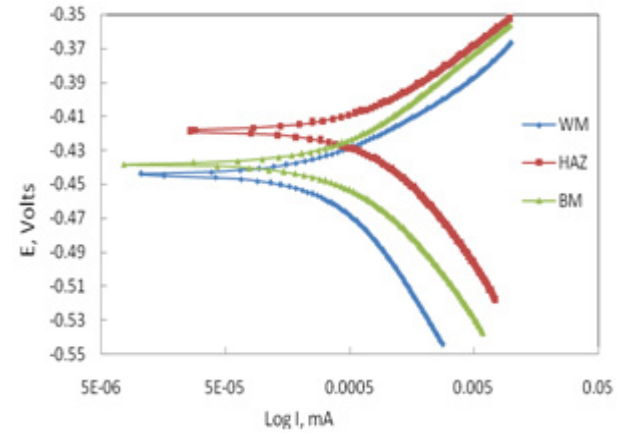

(a)

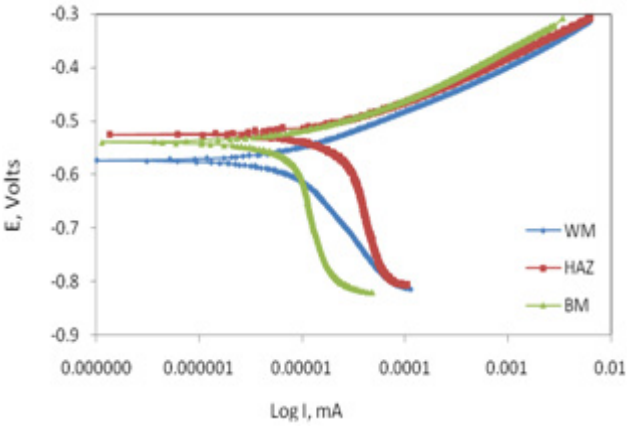

(b)

Figure 4. Potentiodynamic polarization curves for welded steel samples in 1M H_2SO_4 (a) and 3.5% NaCl (b) solutions at room temperature [Blue-WM, Red-HAZ & Green BM]

Table 2. Potentiodynamic polarization parameters of Spiral welded specimens in 1M H_2SO_4 and 3.5% NaCl at room temperature.

Tafel Data						LPP Data
Solution	Material	b_a (mV/decade)	b_c (mV/decade)	E_{corr} (mV)	I_{corr} (µA)	R_p Ω
1M H_2SO_4	WM	40.45	26.65	-444	129.82	53.74
	HAZ	40.86	33.03	-418	297.45	26.62
	BM	31.46	24.40	-438	141.82	42.08
3.5% NaCl	WM	60.11	37.57	-576	2.451	4098.7
	HAZ	34.25	22.71	-526	3.332	1949.3
	BM	46.43	36.57	-539	2.638	2172.8

The polarization curves for welded steel specimens (WM, HAZ and BM) in 1M H_2SO_4 and 3.5% NaCl solution at room temperature are shown in Figs. 4a and 4b for base metal sample. Polarization parameters obtained from the curves are presented in Table 2. These parameters include the values of corrosion current densities (I_{corr}), corrosion potential (E_{corr}), cathodic Tafel slope (b_c), anodic Tafel slope (b_a) and polarization resistance (R_p). The corrosion current density, i_{corr}, was determined graphically for all by extrapolating the cathodic and anodic Tafel slopes to the E_{corr} (versus Ag/AgCl). From the slope analysis of the linear polarization curves in the vicinity of corrosion potential, the values of polarization resistance (R_p) in acid and NaCl solution were obtained.

3.3. Electrochemical Impedance Spectroscopy (EIS) Study

The corrosion response of welded specimens in 1M H_2SO_4 and 3.5% NaCl solution was investigated using Electrochemical Impedance Spectroscopy at room temperature and Nyquist plots represented in the Figs. 5a and 5b and corresponding Bode plots are shown in Figs.6a and 6b for base metal sample. The EIS parameters such as R_{ct}, R_s and CPE_{dl} for both the solutions are listed in Table 3.

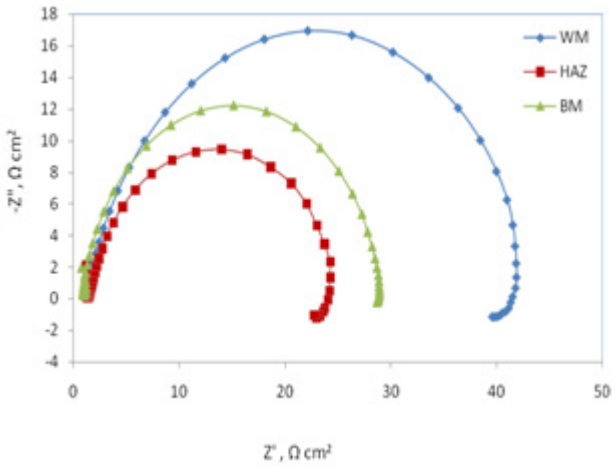

(a)

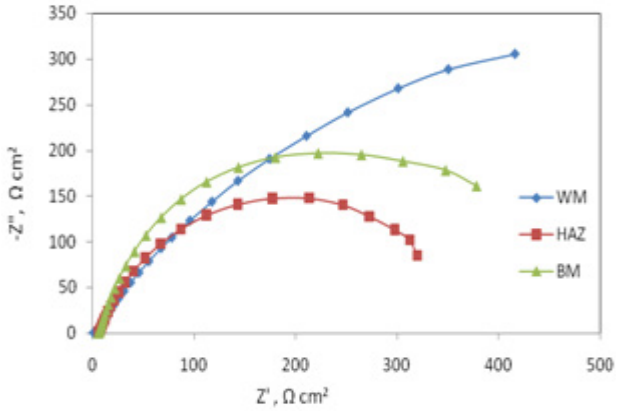

(b)

Figure 5. Electrochemical Impedance curves (Nyquist plot] of welded samples immersed in 1M H_2SO_4 (a) and 3.5% NaCl (b)solutions at room temperature [Blue-WM, Red-HAZ & Green BM].

Table 3. Electrochemical Impedance parameters of Spiral welded specimens in 1M H_2SO_4 and 3.5% NaCl at room temperature.

		R_s (Ω)	CPE (µMho)	n	R_{ct} (Ω)
1M H_2SO_4	WM	1.2	202	0.862	42.0
	HAZ	1.5	255	0.845	23.8
	BM	1	120	0.933	27.8
3.5% NaCl	WM	8	1.91	0.703	990
	HAZ	8	0.597	0.827	340
	BM	10	1.08	0.863	775

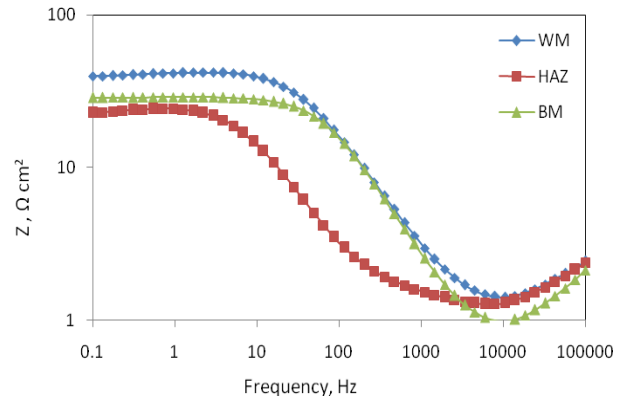

(a)

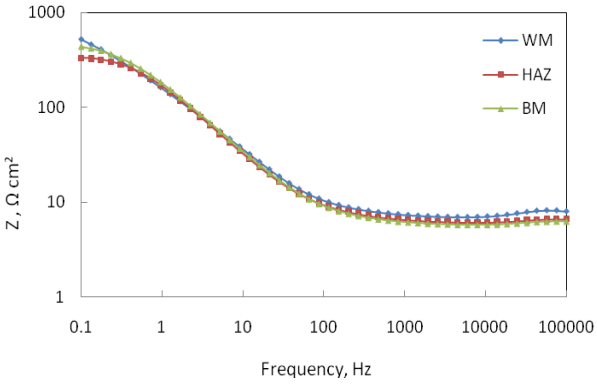

(b)

Figure 6. Bode plot for welded steel samples immersed in 1M H_2SO_4 (a) and 3.5% NaCl (b) solutions at room temperature [Blue-WM, Red-HAZ & Green BM].

4. Discussion

4.1. Effect of Microstructure/grain Size on Corrosion of Welded Steel

From polarization curves (Fig.4) and data from Table 2, it was found that, E_{corr} (versus Ag/AgCl) values of HAZ shifted towards more anodic (positive) region and I_{corr} values of HAZ increases compared to BM and WM. The same corrosion resistance trend was discovered with both the acid corrosion and NaCl corrosion in the following order: WM - BM - HAZ. The coarse grains, residual stresses due to shrinkage, their corresponding lattice strains and the disordered crystals in HAZ all of which favor the formation of microcell corrosion, hence, the corrosion rate of the HAZ is maximum in each corrosive media. Obviously, the corrosion sensitivity is related to the microstructure. The corrosion rate values were lower for the WM and BM which presented an acicular ferrite and ferritic-pearlitic microstructure respectively, whereas, the microstructural analysis showed that the supercritical coarse-grained HAZ and also the supercritical fine-grained HAZ were composed primarily of bainitic- ferrite matrix and suffered a severe localized attack. This is in agreement with the fact that the highest calculated corrosion rate values were obtained for the HAZ. Similar results were obtained by the work of Garcia et al [23], who studied the H_2S corrosion resistance of microalloyed steel with three different heat treatments and microstructures. They observed lower corrosion rate values with acicular ferrite microstructure compared to the values obtained for the ferritic-bainitic and martensitic microstructures [23].

It is seen from these figure that the shapes of Nyquist plot of the WM, HAZ as well as BM specimens are similar at each concentration, with one depressed semicircle indicating that the corrosion mechanism is similar for all regions. As can be seen from these figures, the Nyquist plots don't yield perfect semicircles as expected from the theory of EIS. The deviation from ideal semicircle is generally attributed to the frequency dispersion [24] as well as to the inhomogenities of the surface and mass transport resistant [25]. It is evident from the plots that the impedance response of HAZ specimens showed a noticeable difference compared to BM and WM samples. The capacitance loop intersects the real axis at higher and lower frequencies. At high frequency end, the intercept corresponds to the solution resistance (R_s) and at lower frequency end corresponds to the sum of R_s and charge transfer resistance (R_{ct}). The difference between the two values gives R_{ct} [$(R_s + R_{ct}) - R_s$]. The value of R_{ct} is a measure of electron transfer across the exposed area of the metal surface and it is inversely proportional to rate of corrosion [26]. The smallest capacitive loop in high frequency range is noticed in HAZ than BM and WM for both solutions, which reveals the highest corrosion rate for HAZ steel.

Impedance behavior can be well explained by pure electric models that could verify and enable to calculate numerical values corresponding to the physical and chemical properties of electrochemical system under examination [27]. The simple equivalent circuit that fit to many electrochemical systems consisting of a parallel combination of a double layer capacitance (C_{dl}) and the charge transfer resistance (R_{ct}) corresponding to the corrosion reaction at metal/electrolyte interface and the solution resistance (R_s) between the working and reference electrode [28, 29]. To reduce the effects due to surface irregularities of metal, constant phase element (CPE) is introduced into the circuit instead of a pure double layer capacitance which gives more accurate fit [30] as shown in the Fig. 7.

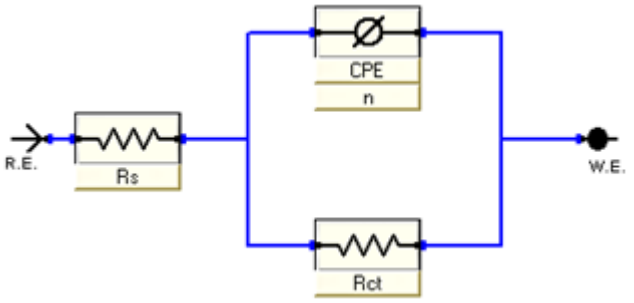

Figure 7. Equivalent circuit fitting for EIS.

The impedance of CPE can be expressed as $Z_{CPE}=1/\ Y_0\ (j\omega)$, where Y_0 is the magnitude of CPE, n is the exponent (phase shift), ω is the angular frequency and j is the imaginary unit. CPE may be resistance, capacitance and inductance depending upon the values of n [28]. In all experiments the observed value of n ranges between 0.8 and 1.0, suggesting the capacitive response of CPE.

From Table 3, the EIS parameters indicate that the values of R_{ct} are less for HAZ than that of BM and WM for both solutions. Bode plots shown in Fig.6 indicates the presence of one time constant, corresponding to one depressed semicircle that obtained in case of Nyquist plots. The total impedance value of HAZ seen in Bode profile is the lowest

one for both solutions.

The corrosion resistance calculated from EIS results shows the same trend as those obtained from polarization measurements. The difference in corrosion resistance of the two methods may be due to the different surface status of the electrode in two measurements [31].

4.2. Corrosion Mechanism (SEM Micrographs and EDX Analysis)

The SEM images of the polished carbon steel surface and those of the corroded surfaces in 1 **M** H_2SO_4 and 3.5% NaCl are shown in Fig.8a, Fig. 8b and Fig. 8c, respectively.

The corrosion products formed on steel surface was analyzed using energy dispersive X-ray analyzer (EDX) as shown in Fig. 9.

The SEM image of polished BM sample in Fig. 8(a) shows a good surface property, while the image in case of corroded welded sample immersed in 1M H_2SO_4 solution was failed because it is severely weakened by external corrosion as shown in Fig. 8(b). The surface shows a homogeneous corroded area with a pile-up of regular crystals, but the surface film is very loose. The corresponding energy dispersive X-ray analyzer (EDX) profiles that were taken for both the images are respectively shown in Fig. 9a and 9b. The atomic percentages of the elements found in polished steel surface indicated that this area were 8.56% C, 89.35 % Fe, 1.04% Mn, 0.60% Si, 0.13% Cr, 0.22% Al, 0.09 % Nb, and 0.15% Mo (Fig. 9a). The atomic percentages of the elements found in corroded surface indicated that this area were 28.82% C, 69.46 % Fe, 1.08% Mn, 0.11% Ti, 0.1% Cr, 0.19 % Nb, and 0.15% Mo (Fig. 9b). The spectra show that Fe peaks are considerably suppressed in the acid solution which is due to dissolution of Fe in acid solution. It has been reported [32] that the cathodic reaction for metals and alloys in sulfuric acid solutions is the hydrogen evolution according to the following equation:

$$2H^+ + 2e^- = H_2 \qquad \text{(Eq.1)}$$

The electrons consumed at the cathode due to the hydrogen ion reduction are produced during the dissolution of iron of the alloy in the corrosive acid medium through the anodic reaction as follows:

$$Fe = Fe^{2+} + 2e^- \qquad \text{(Eq.2)}$$

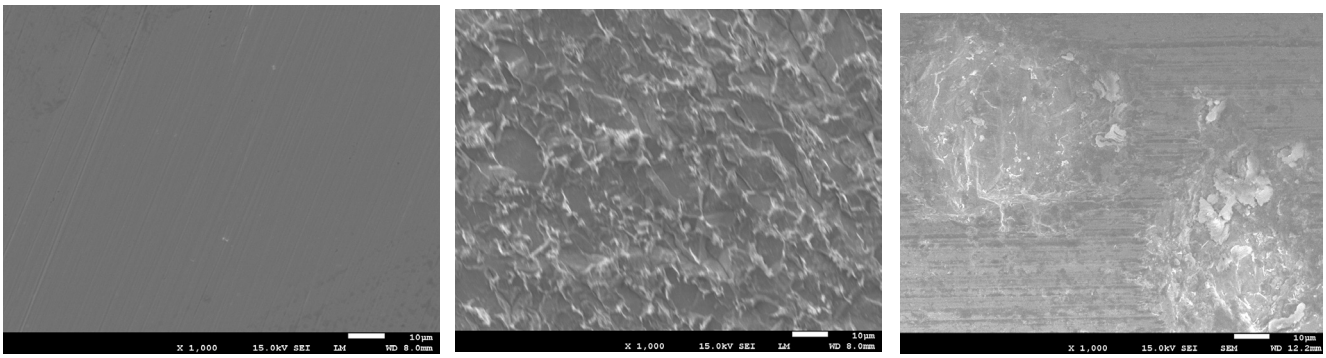

(a) (b) (c)

Figure 8. SEM images of welded (BM) steel (a) before corrosion (b) after corrosion in 1 **M** H_2SO_4 (c) after corrosion in 3.5% NaCl.

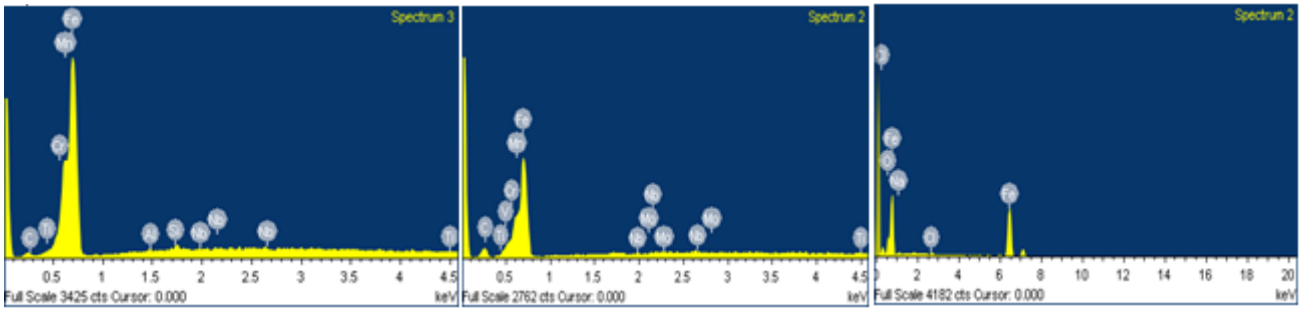

(a) (b) (c)

Figure 9. EDX spectra of welded (BM) steel (a) before corrosion (b) after corrosion in 1 **M** H_2SO_4 (c) after corrosion in 3.5% NaCl.

The image of corroded steel surface in NaCl solution shows a corrosion product developed on the steel surface as shown in Fig. 8c. The atomic percentages of the elements presented on the surface product by salt solution (Fig. 9c) were 18.70% O, 77.50 % Fe, 2.69% Na, and 1.12% Cl. The EDX results from the present study suggest that the better corrosion resistance of alloys in salt solution than acidic might be due to the formation the corrosion product, Fe $(OH)_2$ on metal surface. The spectra show also that Fe peaks are considerably suppressed in the salt solution which is due to the overlying corrosion product. This has been explained on the basis of formation of a protective hydroxide film as represented by the following electrochemical reactions [33]:

Under deaerated condition, the anodic reaction is represented as follows:

$$Fe \rightarrow Fe^{2+} + 2e^{-} \quad \text{(Eq.3)}$$

The cathodic reaction at neutral pH is

$$2H_2O + 2e^{-} \rightarrow H_2 + 2OH^{-} \quad \text{(Eq.4)}$$

Fe^{2+} hydrolysis to form $Fe(OH)_2$

$$Fe^{2+} + 2H_2O \rightarrow Fe(OH)_2 + 2H^{+} \quad \text{(Eq.5)}$$

Under deaerated condition, the corrosion product, $Fe(OH)_2$ formed on metal surface.

SEM/EDX investigations thus confirm the polarization data of the welded steel in salt and acidic solution.

4. Conclusions

The paper aims to understand the corrosion behavior of the weld metal, heat affected zone (HAZ) and base metal of spiral welded pipeline steel at ambient temperature in 3.5% NaCl and 1M H_2SO_4 solution. The grain size is coarse and the assignment is disordered in HAZ by comparing the metallurgical structures of WM and BM. The corrosion rate order of the three regions in the weldment follows the rule as: HAZ > MW > BM. The corrosion resistance, calculated from EIS results, shows the same trend as those obtained from polarization measurements. The corrosion of welded steel in sulfuric acid solution is more due to the dissolution of welded steel under the aggressiveness action of the sulfuric acid solution whereas in NaCl solution, the results have confirmed that the corrosion rates of welded steel is less due to develop a layer of corrosion products and/or oxides that protect its surface.

Acknowledgements

The authors extend their appreciation to the Center of Excellence for Research in Engineering Materials (CEREM) of Advanced Manufacturing Institute, King Saud University, Riyadh, Saudi Arabia for funding the work.

REFERENCES

[1] T. Senthilkumar and T. K. Ajiboye: Journal of Minerals and Materials Characterization and Engineering, 11 (2012) 143-152.

[2] Y.S. Sang, B. Hwang, S. Lee, J. K. Nack, and S.A. Seong: Materials Science and Engineering A, Vol. 458,2007, pp. 281-289.

[3] K. Khulka and S. Aleksandrov: Metallurgist, 50 (2006) 137-143.

[4] A. Bellaouchou, A. Guenbour, A. Ben Bachir: Corrosion 49 (1993) 656-662.

[5] H. Iken, R. Basseguy, A. Guenbour , A. Ben Bachir: Electrochimica Acta 52 (2007) 2580-2587.

[6] T. Poornima, Jagannath Nayak, A. Nityananda Shetty: Portugaliae Electrochimica Acta 28 (2010) 173–188.

[7] A. Guenbour, J. Faucheu, A. Ben Bachir, F. Dabosi, N. Bui.: Corrosion Journal 23 (1988) 4.

[8] A. Guenbour ,M.A Hajji ,E.M. Jallouli , A.Ben Bachir: Applied Surface Science 253 (2006) 2362-2366.

[9] A. Bellaouchou, B. Kabkab, A. Guenbour, A. Ben Bachir: Progress in Organic Coatings 41 (2001) 127-132.

[10] R. Leiva Garcia, M.J. Muñoz Portero, J. Garcia Antón: International Journal of Electrochemical Science 6 (2011) 442-460.

[11] E. Folkhard: Welding metallurgy of stainless steels, Springer, Viena, (1988).

[12] J.A. Brooks, A.W. Thompson, J. Williams: Welding Journal 34 (1984) 71-83.

[13] T. Hemmingsten, H.Hovdan, P. Sanni, N.O.Aagotnes: Electrochimica Acta 47 (2002) 3949-3955.

[14] Kyung-Man Moon, Myung-Hoon Lee, Ki-Joon Kim, Seong-Jong Kim: Surface and Coatings Technology 169-170 (2003) 675-678.

[15] A.B.M. Mujibur Rahman, S. Kumar and A.R. Gerson: Corrosion Science 49 (2007) 4339-4351.

[16] S. Natarajan and S.P. KumareshBabu: Materials Science and Engineering A 432 (2006) 47-51.

[17] Y. Cui and Carl D. Lundin: Materials Letters 59 (2005) 1542-1546.

[18] E. Blasco-Tamarit, A. Igual-Munoz, J. Garcia-Anton, D. Garcia-Garcia: Corrosion Science, 48 (2006) 863–886.

[19] C-M.Lee, S.Bond & P.Woollin: Corrosion (2005) Paper 05277, (Houston, Texas:NACE International, 2005).

[20] E.Gulbrandsen & A.Dugstad: Corrosion (2005) Paper 05276,(Houston, Texas: NACE International, 2005).

[21] F.Martin, C.Garcia, P.Tiedra, Y.Blanco & M.Lopez: Corrosion Engineering Science and Technology 43 (2008) 343-352.

[22] G.Garcia, M.P.de Tiedra, Y.Blanco, O.Martin & F.Martin: Corrosion Science 50 (2008) 2390-2397.

[23] M.A. Lucio-Garcia, J. G. Gonzalez-Rodriguez and M. Casales: Corros. Sci, 51 (2009) 2380-2386.

[24] H. H. Hassan, E.Abdelghani and M. A.Amin: Electrochimica Acta 52 (2007) 6359-6366.

[25] P. Bommersbach , C. Alemany-Dumont, J.P. Millet and B. Normand: Electrochimica Acta, 51 (2005) 1076-1084.

[26] I.L Rosenfield, Corrosion Inhibitors (McGraw-Hill, New York, p.66) (1981).

[27] A. R.Sathiya Priya, V. S. Muralidharan and A. Subramania: Corrosion 64 (2008) 541-552.

[28] A. K. Singh, S. K. Shukla, M. Singh and M.A. Quraishi: Materials Chemistry and Physics 129 (2011) 68-76.

[29] El Azhar M., Mernari B., Traisnel M., Bentiss F.and Lagrenée M.: Corrosion Science 43 (2001) 2229-2238.

[30] J.R. Macdonald and W.B. Johnson: Theory in impedance Spectroscopy, (John Wiley & Sons, New York) (1987).

[31] A. Raman and P. Labine: Reviews on Corrosion Inhibitor Science and Technology,(vol. 1, NACE, Houston, TX , 5) (1986).

[32] E.-S. M. Sherif: International Journal of Electrochemical Science, 6 (2011) 2284–2298.

[33] F. Farelas, A. Ramirez: Int. J. Electrochem. Sci., 5 (2010) 797.